Journal Title
XX(X):1–12

DOI: 10.1177/ToBeAssigned
www.sagepub.com/
SAGE

Morphologically Induced Stability on an Underwater Legged Robot with a Deformable Body

Giacomo Picardi[1], Helmut Hauser[2], Cecilia Laschi[1] and Marcello Calisti[1]

Abstract

For robots to navigate successfully in the real-world, unstructured environment adaptability is a prerequisite. While this is typically implemented within the control layer, there have been recent proposals of adaptation through a morphing of the body. However, the successful demonstration of this approach has mostly been theoretical and in simulations thus far. In this work we present an underwater hopping robot that features a deformable body implemented as a deployable structure which is covered by a soft skin for which it is possible to manually change the body size without altering any other property (e.g. buoyancy or weight). For such a system, we show that it is possible to induce a stable hopping behaviour instead of a fall, by just increasing the body size. We provide a mathematical model that describes the hopping behaviour of the robot under the influence of shape-dependent underwater contributions (drag, buoyancy and added mass) in order to analyse and compare the results obtained. Moreover, we show that for certain conditions, a stable hopping behaviour can only be obtained through changing the morphology of the robot as the controller (i.e. actuator) would already be working at maximum capacity. The presented work demonstrates that, through the exploitation of shape-dependent forces, the dynamics of a system can be modified through altering the morphology of the body to induce a desirable behaviour and, thus, a morphological change can be an effective alternative to the classic control.

Keywords

Morphological Computation, Soft Robotics, Deformable Robot, Legged Locomotion, Underwater Robotics

1 Introduction

Traditional robotics generally aims to design machines capable of fast operations in tasks that require a high degree of precision or force which are impossible to be achieved by humans. To pursue this goal, the design approach typically consists of building machines with rigid body parts and high torque motors, thereby facilitating the modelling and controlling process Pfeifer et al. (2005). As a matter of fact, this approach has produced machines of high performance, and these are mainly employed for manufacture in structured environments, thus minimizing the interaction with humans. However, when a robot needs to operate in a complex, unstructured environment the traditional approach often breaks down. Furthermore, the burden of adaptation is on the controller, a task which often exceeds the available computational capacity and resulting in extremely slow motion planning, with difficult implementations in real world scenarios Guizzo and Ackerman (2015). Although capable of outperforming biological systems in terms of precision and strength, traditional robotics have a tendency to struggle in areas where adaptability, agility and safe interaction with humans and natural environments are in demand. To cope with these new challenges, a new branch of robotics based on biological inspiration is born. At the foundation of this new conception of robotics lies the observation that biological systems evolve their morphology and brain in unison to accomplish specific tasks in specific environments and if we want to get closer to their performance, we would need to follow a similar approach Pfeifer et al. (2007). This idea was beautifully illustrated with the evolution of creature's bodies and brains in simulations Sims (1994); Mautner and Belew (2000), or by co-evolving control and specific sensory systems (i.e. acoustic system) in actual mobile robot Lund and Hallam (1997). One of the cornerstones of this approach would be the concept of Morphological Computation (MC), i.e. the distribution of tasks among the brain (controller), the morphology (shape, materials, sensors, actuators) and the environment Pfeifer et al. (2006). The idea has a wide number of applications within its scope. MC is sometimes referred to as the possibility of using the complex nonlinear dynamics of a deformable body to serve as a computational resource in control tasks Nakajima et al. (2014, 2015); Hauser et al. (2018), with a particular focus on soft manipulators control Nakajima et al. (2013); Eder et al. (2017) and locomotion Zhao et al. (2013). A different branch of MC can be found in the field of robot locomotion, where the interaction with a complex and non-structured environment is not handled by means of complex controllers, but by harnessing the intrinsic properties of

[1]The BioRobotics Institute, Scuola Superiore Sant'Anna, Viale Rinaldo Piaggio 34, 56025, Pontedera (PI), Italy
[2]University of Bristol and University of the West of England, Bristol, BS16 1QY, U.K.

Corresponding author:
Giacomo Picardi, The BioRobotics Institute, Scuola Superiore Sant'Anna, Viale Rinaldo Piaggio 34, 56025, Pontedera (PI), Italy
Email: giacomo.picardi@santannapisa.it

the materials used in construction Auerbach and Bongard (2017); Calisti et al. (2017). Examples of such instances include the exploitation of elastic elements in dynamic legged locomotion to produce self-stabilising gaits Iida and Pfeifer (2004), or in flapping flight to exploit the resonant frequency of the system Ma et al. (2013); and the careful design of variable stiffness profiles for artificial wings and fins to distribute the load and optimize fluid dynamics properties of the robots Jun et al. (2008); Zhao et al. (2010), or to produce rich movements with the need for minimal control Shepherd et al. (2011); Marchese et al. (2014). Overall, the concept of MC suggests that it can be beneficial to outsource functionality to morphological features. A disadvantage of this approach would be that functionality is tied to a fixed morphology. However, a solution has recently been proposed. The idea is to exploit variable morphology often referred to as a morphosis Hauser and Corucci (2017). This results in an enhanced adaptability of robots Pfeifer et al. (2007); Laschi et al. (2016) and the increased robustness of evolved behaviour Bongard (2011). Furthermore, it has been shown in simulations that is possible to induce different gaits on a passive bipedal walker through just modulating the stiffness of the knee and hip joints Owaki et al. (2008). In Corucci et al. (2015b,a), an evolutionary approach was applied within the simulation to study how a soft underwater robot can be adapted to perform in different kinds of locomotion by changing the shape of its body. Specifically, the authors were able to show that it is possible to switch from legged locomotion to swimming functionality by changing just one morphological parameter. Similarly, it has been shown that the evolution of legged gaits in a population of robots is more robust in cases where their morphology gradually transitioned from anguilliform into legged, particularly when compared to a population that did not transition through the anguilliform body plan Bongard (2011). There also has been an attempt to mathematically formalize MC in the context of adaptive morphology Füchslin et al. (2013). The authors aimed at creating a framework in which the effects of a morphological change can be described in terms of modifications of the attractors landscape of the system. Aside from these interesting insights, there has been very little experimental work on real robots and in showing the potential of adapting morphologies to control behaviours. For example, Vu et al. (2013) demonstrated that systematically changing the stiffness would be able to increase energy efficiency in locomotion. However, their work was constrained to 2D hopping. Garrad et al. (2018) demonstrated that it is possible to change the behaviour of a four-link pendulum which would be driven by a single actuator not only by controlling it with different oscillation frequencies and amplitudes, but also by tuning the stiffness of four springs placed at each non actuated joint. Their setup was designed with locomotion in mind, but no results on that have been published so far. In this work, we will show how adaptive morphology can improve and extend locomotion behaviour in an underwater legged robot. We employ a framework introduced in Calisti et al. (2016), which uses an actuated spring loaded inverted pendulum model to describe underwater locomotion. The system was chosen for two main reasons. Firstly, this system has two attractors that result in two different behaviour*. The system can either converge to a limit cycle, which corresponds to a hopping behaviour (desirable) or to a fixed point corresponding to a fall, which should be prevented. Secondly, by being underwater, the system is strongly influenced by shape-dependent contributions, such as drag and added mass. This allows us to highlight body-environment interactions, which are at the core of MC. The intuition that altering the morphology of this particular platform could have a critic effect on the behaviour is based on results from Calisti and Laschi (2018). Extensive simulations of underwater spring loaded inverted pendulum (U-SLIP) models, introduced in Calisti and Laschi (2015), suggest that shape-related parameters influence the stability of the system. The goal of this paper is to experimentally validate this and, therefore, form a more general perspective. The idea is to provide experimental evidence that it is possible for a complex dynamical system, like this underwater robot, to control behaviour by means of morphological changes. In order to put the results that were obtained into a more general context, the observed phenomenon is analysed in terms of the attractors landscapes and their dependencies on morphological parameters, as suggested by the theoretical work found in Füchslin et al. (2013). Moreover, the influence of body-environment interactions on the dynamics of the robot is characterized and discussed with the aid of the U-SLIP model. Finally, it should be pointed out that in the case of the presented experiments, the desired behaviour could not be induced by classic control, as the actuator was already working at its maximum capacity. The proposed MC approach is not only an elegant alternative for solving a control problem, but also allows an extension of the space of possible behaviours.

2 Materials and Methods

2.1 Experimental Setup

The results presented in this work are obtained using the setup depicted in Fig.1. The core of the experimental setup is a single-legged robot which exhibits hopping locomotion in a water filled tank (dimensions $60x60x120cm$), similar to the one presented in Calisti et al. (2016). A CAD of the robot showing all relevant components is reported in Fig. 2. The leg of the robot features a linear spring ($k = 140N/m$) in series with an elongation mechanism implemented as a crank slider and actuated by a servomotor (HS-5086WP, Hitech). The action of the servomotor is triggered by a contact sensor (FSR 400 Short 5mm Circle x 20mm, Interlinks Electronics), conveniently embedded in silicone to make it waterproof, and lodged in the distal part of the leg, namely the *foot*. The rotation of the leg around its orientation axis is constrained by a pin (not shown in the figure) which defines the leg touchdown angle. The position of the pin can be manually regulated to obtain different touchdown angles. However, in the work presented, it was kept at 82° with respect to the ground. On top of the leg, a spherical deployable mechanism is covered with a silicone (Ecoflex 0030) skin, namely the *head*, which allows switching between a small

*This is consistent with the framework suggested by Füchslin et al. (2013)

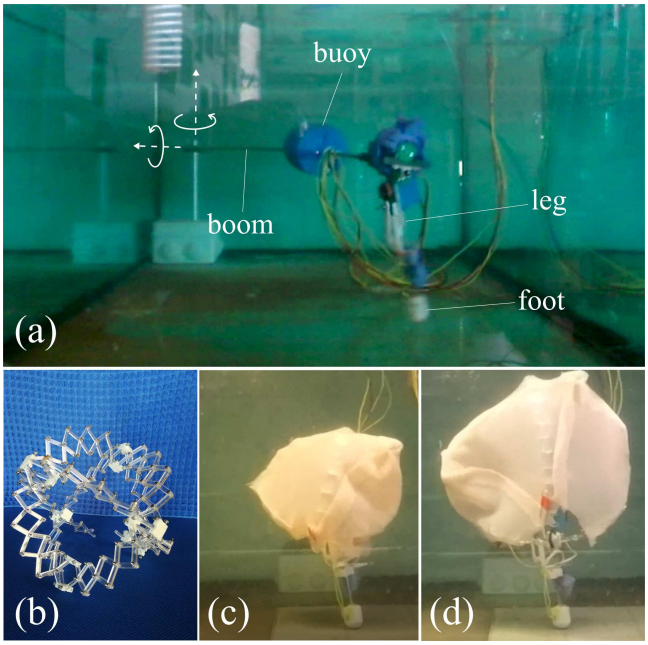

Figure 1. Experimental setup. A) The robot is operated in a tank, supported by a boom that allows two rotational degrees of freedom. A foam cylinder (buoy) can be moved along the boom to regulate the net vertical force acting on the system. B) The spherical deployable mechanism used to vary the size of the head. C,D) The robot featuring small and big head.

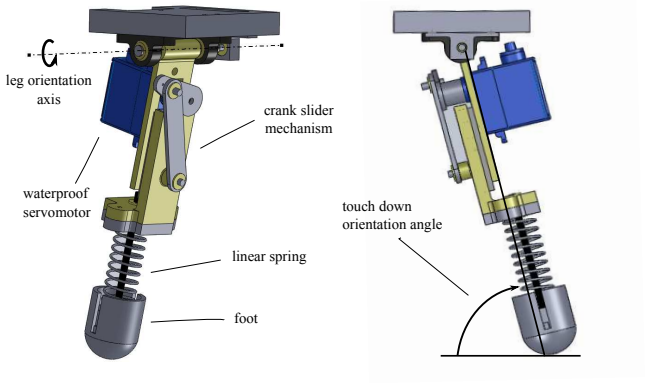

Figure 2. A CAD sketch of the robot.

head (6.3cm radius, Fig. 1c) and a big head (9cm radius, Fig.1d) configuration without altering any other properties of the system (e.g. dry mass, buoyancy). The presented setup does not allow online modifications of the head size, which is outside of the scope of the paper. The overall dry mass of the robot, as measured on a scale outside water, including the head, weighed at 0.7135kg. As commonly done when evaluating single-legged hopping machines, the motion of the robot is constrained by a support system made of a boom (Brown and Zeglin (1998)) that allows two rotational degrees of freedom (Fig. 1a). The centre of mass of the robot is therefore moving on a spherical surface. However, given the ratio between the length of the boom ($81cm$) and the leg of the robot ($19cm$), the system can be considered to be moving on a vertical plane without altering the analysis and discussion presented. In addition, the vertical net force acting on the system can be regulated by moving a foam cylinder (buoy) along the boom. Selecting the system configuration desired Q (buoy position and head size), a trial began with the robot being manually released in the water and beginning to fall. When the foot gets in contact with the ground (*touchdown event*) the spring starts to compress, due to the inertia of the system. The detection of the contact triggers the action of the servomotor that elongates the crank slider, resulting in further compression of the spring. Similarly, the leg is free to pivot backward until the elastic force acting on the spring exceeds the other contributions and the system detaches from the ground again (*lift-off event*). When the system is not in contact with the ground, the leg passively rotates back to the touchdown angle defined by the position of the pin. Given the selected configuration, a trial might result in the robot falling or periodically hopping until it reaches the end of the tank. In the text, we will sometimes refer to these two outcomes respectively as unstable or stable trials (configurations).

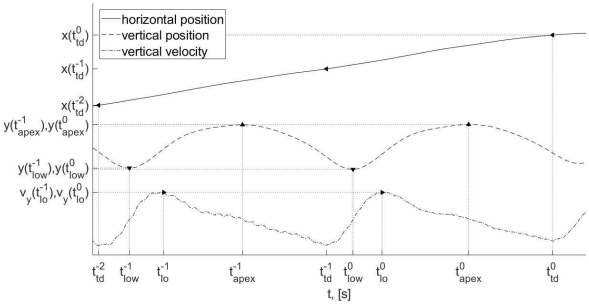

Figure 3. Example of horizontal and vertical position, and vertical velocity trajectories with events relevant to the calculation of the statistics presented in the Results section. Events on the plot are marked as follows: ◄ - touch down events (td), ► - lift off events (lo), ▲ - apex events (apex), ▼ - lowest vertical position events (low). The superscript i is the i-th event before the last.

Experiments were filmed using a GoPro Hero 4 at 120fps, with a spatial resolution of 1280x720 pixels. For each trial, the position trajectories x and y of a red marker placed on the silicone skin were extracted using the open source software Kinovea and subsequently imported in MATLAB. Trajectories x and y were low-pass filtered using Savitsky-Golay filter (order = 3, frame length = 91) and were differentiated with respect to time to obtain velocity trajectories v_x and v_y. An example of the trajectories obtained from the tracking is shown in Fig. 3, along with the time steps of significant events. In particular, the time steps of *apex* and *lowest vertical position* events (t_{apex}, t_{low}) were extracted as local maxima and minima points of y, whereas the time steps of *lift-off* and *touchdown* events (t_{lo}, t_{td}) were respectively extracted as maxima and minima points of v_y. It is to be noted that, by definition *lift-off* and *touchdown*, events correspond to the time steps at which the system respectively detaches and gets in contact with the ground. However, the operative definition used in the data analysis did not differ much in practice and allowed the automatic identification of such events. For each stable trial, the periodic motion of the system can be described by four statistics, namely *locomotion features*, i.e. horizontal velocity, lift off vertical velocity, vertical

excursion, and hopping frequency, here indicated as the set $S = \{v_x, v_y^{lo}, \Delta y, f\}$. The locomotion features were calculated as functions of the event extracted from the last $N = 2$ hops, and are as follows:

- horizontal velocity, $v_x = \frac{x(t_{td}^0) - x(t_{td}^{-N})}{t_{td}^0 - t_{td}^{-N}}$
- lift off vertical velocity, $v_y^{lo} = \frac{1}{N} \sum_{i=-(N-1)}^{0} v_y(t_{lo}^i)$
- vertical excursion, $\Delta y = \sum_{i=-(N-1)}^{0} y(t_{apex}^i) - y(t_{low}^i)$
- hopping frequency, $f = \frac{N}{t_{td}^0 - t_{td}^{-N}}$

The locomotion features extracted from trials obtained with the same configuration Q can be averaged to obtain the mean locomotion features $S_Q = \{\overline{v_x}, \overline{v_y^{lo}}, \overline{\Delta y}, \overline{f}\}$.

2.2 U-SLIP model

The hopping locomotion of the robot presented in section 2.1 can be described with a two dimensional model depicted in Fig. 4. Such model was introduced for the first time in Calisti and Laschi (2015) and extends the Spring Loaded Inverted Pendulum (SLIP) template (Blickhan (1989)) by considering the contributions of the underwater environment (i.e. hydrodynamic drag, added mass and buoyancy) and a linear actuator in series with the spring. For this reason, the model takes the name of Underwater Spring Loaded Inverted Pendulum (U-SLIP). For the readers' convenience, we will summarize the essentials of U-SLIP and detail how the model was used within the presented work in the following section.

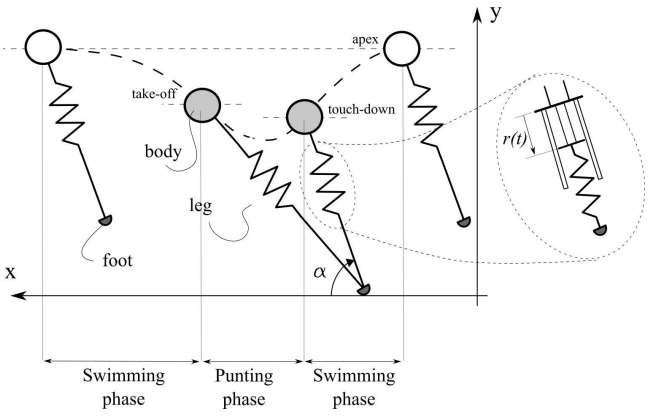

Figure 4. The U-SLIP model is made of a point-mass body subjected to hydrodynamic forces, and a massless leg which can be radially elongated upon contact. Two phases are distinguished: a punting phase and a swimming phase.

The equations describing the horizontal and vertical dynamics of U-SLIP are reported in Eq. 1,

$$\begin{cases} \ddot{x} = -\frac{X}{m+M}\dot{x}|\dot{x}| + \frac{k(x-x_t)}{m+M}\left(\frac{(r_0+r)-l}{l}\right) \\ \ddot{y} = -\frac{Y}{m+M}\dot{y}|\dot{y}| - \frac{mg}{m+M} + \frac{\rho_w V g}{m+M} + \frac{ky}{m+M}\left(\frac{(r_0+r)-l}{l}\right) \end{cases} \quad (1)$$

where $l = \sqrt{(x-x_t)^2 + y^2}$, $X = \frac{1}{2}A_x\mu_x\rho_w$, $Y = \frac{1}{2}A_y\mu_y\rho_w$, $V = V_r + dV$ and all variables and parameters are reported in Tab. 1. The dynamics of U-SLIP are divided into *punting phases*, which occur whenever the foot is in contact with the ground, and *swimming phases*.

Table 1. Variables and Parameters of U-SLIP model. Configuration independent parameters are chosen by design or are physical constants. Configuration dependent parameters vary either with head size or with buoy position. Notice that the volume and mass of the robot (V_r and m) are independent from the head size as the increased amount of water carried along would be accounted for by the added mass term M.

Variables	
x	CoM horizontal position
$\dot{x}$	CoM horizontal velocity
y	CoM vertical position
$\dot{y}$	CoM vertical velocity
l	leg length
x_t	horizontal foot position
r	leg elongation (input)
α	leg orientation (input)

Control Parameters		Value
r_s	elongation speed	$2.93cm/s$
α_{td}	leg orientation at touch down	82°

Configuration independent parameters		Value
m	dry mass	0.7135Kg
r_0	rest leg length	19cm
Δr	maximum elongation	2cm
V_r	volume of the robot	$4.5478 \cdot 10^{-4}$Kg/m^3
k	spring elastic coefficient	140N/m
g	gravity constant	9.81m/s^2
ρ_w	water density	1000Kg/m^3

Configuration dependent parameters		Dependence
A_x	x-referenced area	Head size
A_y	y-referenced area	Head size
μ_x	x-drag coefficient	Head size
μ_y	y-drag coefficient	Head size
M	added mass	Head size
dV	dummy volume	Buoy position

During the swimming phases, the system is not in contact with the ground and there is therefore no contribution of elastic force on the dynamics. Mathematically, this can be expressed in Eq. 1 by setting $k = 0$. The transitions between swimming and punting phases is called *touch down* event and corresponds to the condition $y = lsin(\alpha)$, whereas the transition between punting and swimming phases is called *lift off* event and correspond to the condition of energetic balance on the spring, expressed by $l = r_0 + r$. The inputs of the system are the leg elongation r and the leg orientation α. The control law that were employed consists in elongating the leg with constant velocity r_s during punting phases and resetting the leg orientation at the constant touch down angle α_{td} during swimming phases. Depending on the values of the parameters and the selected initial conditions, the U-SLIP may converge to two attractors, one would be the plane $y = 0$, which corresponds to the fallen condition, and the other is a limit cycle, which corresponds to periodic hopping locomotion. The parameters of U-SLIP, listed in Tab. 1 are divided into configuration independent and configuration dependent. For the robot used in this work, the values of configuration independent parameters

are known and reported in Tab. 1. On the other hand, the values of configuration dependent parameters, which define the interaction between the robot and the underwater environment for different buoy positions and head sizes, are unknown. In particular, changing the position of the buoy along the boom was found to have a predictable effect only on the term of Eq. 1 connected with the buoyancy force. Conversely, changing the head size affects all terms of Eq. 1 because it influences upon all the hydrodynamic parameters (A_x, A_y, μ_x, μ_y and M). The estimation of hydrodynamics parameters is very challenging, particularly in the case of traditional physics-based identification techniques due to the irregular shape of the robot and the trajectories exhibited. For this reason, instead of trying to estimate the configuration dependent parameters as they appear in Tab. 1, we defined the set of four aggregate parameters $P = \{A, B, C, D\}$, as reported in Eq. 2 and applied the following procedure.

$$\begin{aligned} A &= X/(m+M) \\ B &= Y/(m+M) \\ C &= (m-\rho_w V)g/(m+M) \\ D &= k/(m+M) \end{aligned} \tag{2}$$

First, a stable system configuration Q^* (buoy position l_b and small head) is taken as a reference and the set of mean locomotion features extracted from it is named S_*. Then, U-SLIP is simulated several times, with values of aggregate parameters that vary within a span of physically reasonable values (i.e. $A \in [2.5, 35], B \in [2.5, 35], C \in [6.75 \cdot 10^{-4}, 6.75 \cdot 10{-}3], D \in [11.5, 115]$). If the n-th simulation results in stable hopping, the corresponding locomotion features are saved in S_n and so the corresponding set of aggregate parameters P_n. The set of aggregate parameters P_n which minimizes the distance between S_n and S_* ($\sqrt{S_n^2 - S_*^2}$) is selected and named $P_* = \{A_*, B_*, C_*, D_*\}$. Finally, the aggregate parameter C_* can be generalized for any given displacement of the buoy dl from the reference position l_b by means of the simple formula reported in Eq. 3:

$$dC = -\frac{L\rho_w V_b g}{(m+M)} dl \tag{3}$$

where V_b is the volume of the buoy. The derivation of Eq. 3 is reported in the Appendix. The same procedure is repeated for big headed configurations. Finally, it is worth noting that the procedure hereby reported further allows for the identification of aggregate parameters in the case of unstable configurations. This is as the mean locomotion features (which are defined only for stable configurations) are only used to identify the set P_*, which is then generalized to any buoy position (including the ones resulting in unstable motion) by means of geometric derivation, which is further reported on in the Appendix.

3 Results

First, a total of 128 trials were conducted, with 26 different configurations of the system, as summarized in Table 2. Most of the configurations resulted in stable hopping trajectories that reached the end of the tank, whereas some resulted in the robot falling. Thirteen decreasing buoy distances were tested with both head sizes. Regardless of the head size, the system successfully reached the end of the tank for the first nine buoy positions. In the case of the buoy distances 8.7cm and 7.9cm, the system fell for every trial with the small head. Conversely, when it was tested with the big head, while still maintaining all other characteristics as unchanged, the robot successfully reached the end of the tank for all buoy distances. Finally, for buoy positions smaller than 7.9cm, none of the configurations exhibited stable hopping. We noted that we observed a *morphological recover of stability* every time the stability of hopping behaviour was restored through increasing the head size.

Table 2. Configurations of the robot that resulted in a *falling behaviour* are highlighted in red. In two cases, a *hopping behaviour* was restored by increasing the size of the head. These configurations are highlighted in green. Buoy position is the distance from the vertical pivot to the buoy, and the small and big head have radii equal to $6.3cm$ and $9cm$, respectively.

Buoy Position	Head Size	No. of Trials	No. of Successes
20.5cm	Small	5	5
	Big	5	5
19.2cm	Big	5	5
	Small	5	5
17.8cm	Small	5	5
	Big	5	5
16.5cm	Small	5	5
	Big	5	5
15.1cm	Small	5	5
	Big	5	5
13.1cm	Small	5	5
	Big	5	5
12.1cm	Small	5	5
	Big	5	5
10.6cm	Small	5	5
	Big	5	5
9.5cm	Small	5	5
	Big	5	5
8.7cm	Small	3	0
	Big	5	5
7.9cm	Small	5	0
	Big	5	5
7.4cm	Small	5	0
	Big	5	0
6.9cm	Small	5	0
	Big	5	0

The tracking of the centre of mass (CoM) of the robot for which a morphological recover of stability was observed was reported in Fig.5. In unstable hopping conditions (i.e. small head, 8.7cm buoy distance (a) and small head, 7.9cm buoy distance (b)), the robot progressively reduced the height of the subsequent apexes, while increasing its forward tilt. Within a few steps, the robot was unable to reach the touchdown height and eventually fell to the ground. This behaviour was consistently observed for all the trials carried out with the unstable configurations. Once the size of the head was increased (without any modification in the leg angle or elongation speed), a change was observed in the robots behaviour. The tracking of the first step appeared similar to the small-head configuration, but the subsequent

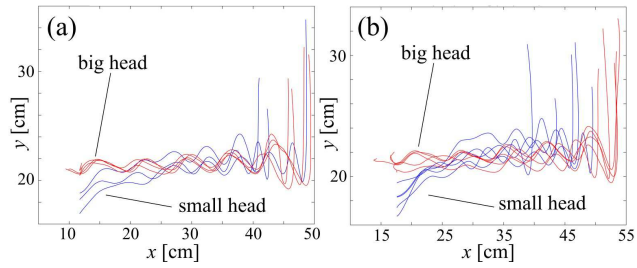

Figure 5. Trajectory tracking of the centre of mass of the robot for buoy position $8.7cm$ (a) and $7.9cm$ (b). Blue lines are used for small head configurations, and red lines are used for big head configurations. For the trials hereby reported, all small head configurations resulted in a fall, whereas big head configurations successfully reached the end of the tank. All tracks are aligned with respect to the last touchdown.

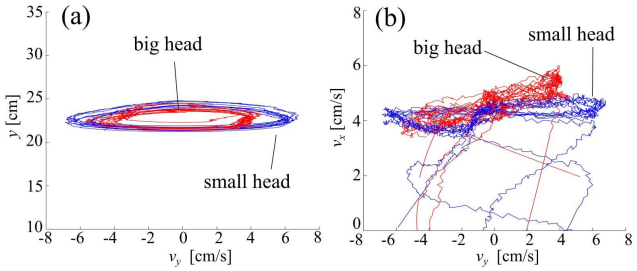

Figure 6. Limit cycle comparison between small (blue) and big (red) head configurations for buoy position $15.1cm$. Increasing the size of the head has the main effect of slowing down the vertical dynamics, while leaving vertical excursion and horizontal velocity practically unchanged, as shown by the $(v_y - y)$ projection plane (a) and the $(v_y - v_x)$, respectively.

Table 3. Experiment outcome for 40 additional trials carried out with a $50g$ lead ballast attached to the robot. The trials are focused only on buoy positions for which the small head configuration exhibits a falling behaviour.

Buoy Position	Head Size	No. of Trials	No. of Successes
16.5cm	Small	10	0
	Big	10	10
15.1cm	Small	10	0
	Big	10	10

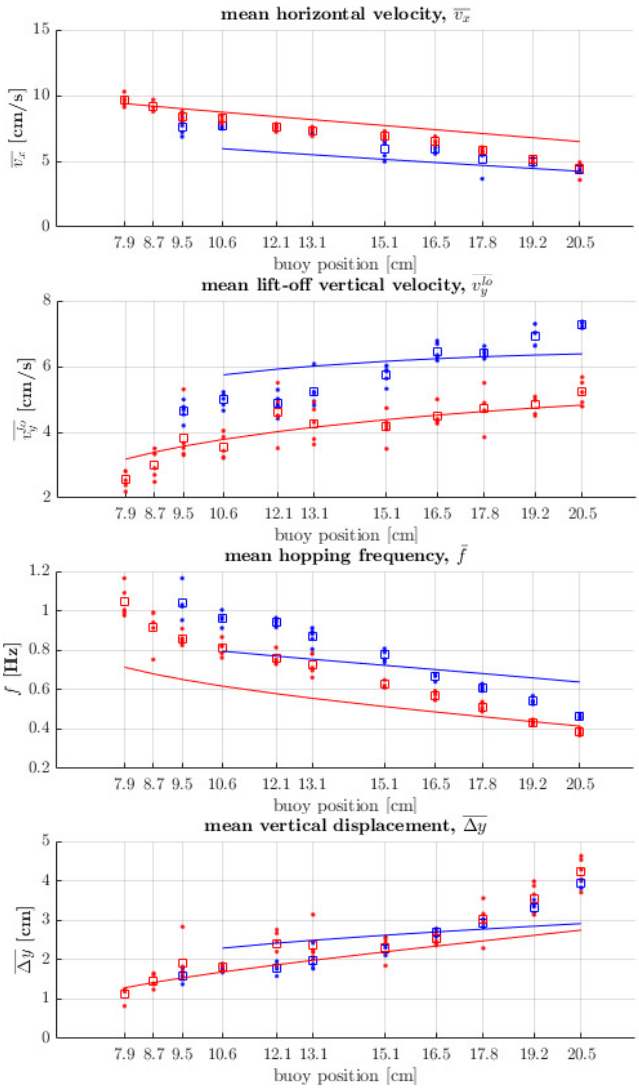

Figure 7. Comparison between locomotion features extracted from experiments and derived with U-SLIP model. Dots represent the observed values of the features set S extracted from the experiments, squares represent the mean value. Blue colour stands for small head, while red colour indicates big head. Solid lines represent the model prediction with respect to the variation of buoy position. Lines and squares are not shown if the robot or the model exhibited an unstable behaviour.

steps differ significantly. In the big-head configurations, the robot was able to keep the height of the apex above the touchdown height until it encountered the end of the tank, thus showing a quasi-periodic behaviour.

In order to confirm that the observed stability recovery did not happen by chance, an additional set of experiments was carried out, as reported in Tab. 3. A 50g lead ballast was attached to the robot to explore a different region of the parameters space. This set of trials is focused only on buoy positions for which the small headed configuration falls, i.e. 16.5cm and 15.1cm. For both buoy positions, the big head configuration successfully reached the end of the tank in all trials, whereas for buoy positions smaller than 15.1, none of the configurations exhibited a stable behaviour.

By analysing the effect of the morphological change on the locomotion of the robot, we observed that the vertical excursion and the horizontal speed were comparable, whereas the maximum vertical speed was significantly lower. This is highlighted by the comparison of the limit cycles shown in Fig.6 (and also reported in Tab.5 in Appendix). The picture reports the limit cycles for the buoy distance to be at 15.1cm, a point where both configurations demonstrated a clearly periodic behaviour. When the head is morphed from the contracted configuration (blue line) to the expanded configuration (red line), no significant change in the vertical excursion was noticed (Fig.6a), nor was it noticed in the mean horizontal velocity (Fig.6b), but the limit cycle significantly shrank with respect to the maximum vertical speed (Fig.6a).

Periodic motion of the hopping system can be described by the set S of locomotion features defined in section 2.1. Both the sizes of the head and position of the buoy influenced S, as shown in Fig.7. By increasing the buoyancy force (or equivalently speaking the buoy distance) $\overline{v_x}$ and $\bar{f}$

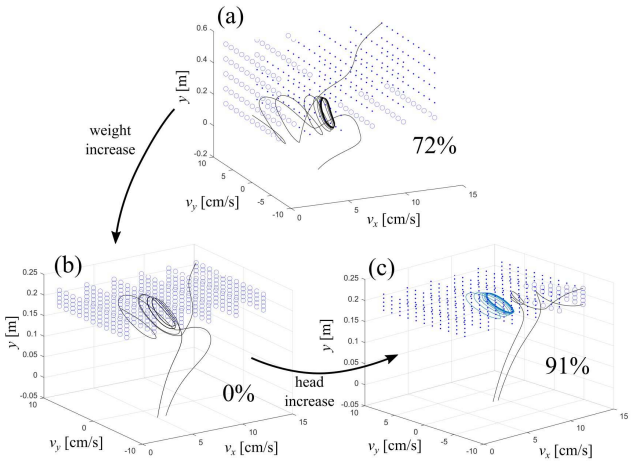

Figure 8. The basins of attraction for different configurations: small head and buoy position 10.6cm (a), small head and buoy position 9.5cm (b), big head and buoy position 9.5cm (a). Initial conditions attracted by the limit cycle are represented by dots, while white circles represented the others. The percentages of stable initial conditions with respect to the spanned rages of initial states are highlighted. For each basin, some stable or unstable trajectories are also shown, except for picture (b), where no stable initial conditions were found.

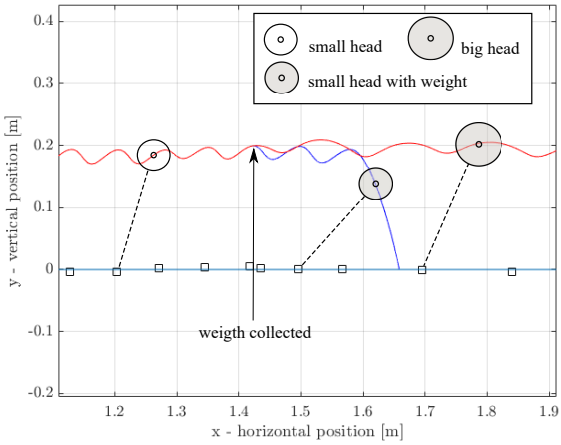

Figure 9. An example of the trajectories of the CoM during uneven ground simulations. The moment when the robot takes the additional weight and the head size is increased is presented. Before the arrow, the robot had no weight and ran on uneven ground; after the arrow the robot had additional weight, and we obtained a falling (blue line) and a running behaviour (red line).

decreased, whereas $\overline{v_y^{lo}}$ and $\overline{\Delta y}$ increased. By increasing the dimension of the head, $\overline{v_x}$ and $\overline{\Delta y}$ were slightly influenced, while $\overline{v_y^{lo}}$ was reduced, along with $\bar{f}$. As explained in the procedure reported in section 2.2, buoy distance of 15.1cm was taken as reference and subsequently the model was used to predict the locomotion features at different buoy positions. The qualitative behaviour of S with respect to buoy distance is correctly replicated, as shown by solid lines in Fig.7. Whenever the model did not reach the limit cycle (i.e. the CoM fall) the line is not displayed. For small headed configurations, the line interrupted at buoy position 10.6cm, inferring that the model did not reach the limit cycle for distances in the range (7.9cm, 9.5cm). On the other hand, for big headed configurations, the model reported a stable hopping behaviour for all buoy distances above 9.5cm. In the small headed configuration, the model appears to underestimate the stability of the real system (Table 2).

Table 4. Average number of step, η_s, out of 100 trials and the associated standard deviation (σ_s) before falls. The data is presented with respect to the different level of asperity of the ground ξ, for the small head (S) and big (B) before and after the collection of a payload.

		Without weight		With weight	
$\xi[cm]$	head	$\eta_s(\sigma_s)$	success	$\eta_s(\sigma_s)$	success
0.5	S	20(0)	100%	20(0)	100%
	B			20(0)	100%
1	S	19.8(0.9)	96%	9.8(7.0)	21%
	B			16.7(7.3)	83%
1.5	S	13.0(5.7)	30%	0.7(1.7)	0%
	B			2.3(5.4)	4%
2	S	8.8(4.4)	5%	0(-)	0%
	B			0(-)	0%

The recovery of the stability reported in this work is the effect of a modification to the basin of attraction of the limit cycle within the system. In particular, an increase of the head size, not only modified the shape of the limit cycles, as shown in Fig. 6, but also increased the volume of their basin of attraction. Consequently, for buoy distances of 8.7cm and 7.9cm, the same initial condition (IC) lies outside the basin of attraction of the limit cycle when the head is small, and inside when the head is big. We resorted to utilizing U-SLIP simulations to estimate the volume of the basins of attraction for three different configurations that were tested on the system (see Fig. 8). For each configuration, we simulated the U-SLIP from a range of realistic IC. IC which resulted in a stable behaviour were marked with a circle, otherwise with a dot. Firstly, for the configuration with small head and buoy position 10.6cm (Fig. 8a) 72% of IC tested resulted in a stable behaviour. Then, in the case of the small head and buoy position 9.5cm (Fig. 8b) the percentage of stable IC drops to zero. Finally, by increasing the head size (buoy position 9.5 and big head) the percentage of stable IC becomes 91% (Fig. 8c). Even though the stability of small headed configuration is slightly underestimated, this result confirms the ability of the model to predict the degree of stability of the system based on different morphologies.

In order to further evaluate the relevance of morphological induced stability in realistic application scenarios, we also performed extensive simulations in uneven ground condition. The hopping behaviour was simulated for twenty initial steps, where the ground height was randomly displaced between $[-\xi/2, \xi/2]$. After twenty steps, a payload of 50g (around 7% of the robot's weight) was added to the robot, and the simulation continued with a small or a big head for an additional twenty steps. The amount of the ground displacement ξ was increased from 0.5cm to 2cm (corresponding approximately to 2.5 to 10% of the leg's length). For each displacement one hundred simulations were performed.

For $\xi = 0.5$cm, the ground asperities were easily negotiated by the robot, for both morphologies, regardless

of the payload (Tab.4). For $\xi = 1$cm, the self-stabilizing behaviour of the robot with small head was severely influenced by the payload, and the success rate of the locomotion dropped to 21% whereas, by increasing the head size, a stable locomotion was obtained in 83% of the runs. An example of recovery for $\xi = 1$cm is shown in Fig.9.

For $\xi = 1.5$ the system without payload was not able to consistently reject the ground disturbances (30% of success rate), and after payload collection only the big head configuration accomplished 40 hops (4% of success rate). Finally, for $\xi =$2cm the asperities were impossible to be negotiated for both morphologies.

4 Discussions

In the previous section, we experimentally documented the ability to induce a stable hopping behaviour by just increasing the head size for four of otherwise unstable system configurations. This possibility was anticipated in the theoretical work Calisti and Laschi (2018),and the hopping stability of U-SLIP model was investigated with respect to variations of four a-dimensional aggregate parameters linked with shape-dependent contributions typical of the underwater environment (i.e. drag, buoyancy and added mass). In particular, it was shown that for a given level of buoyancy, the basin of attraction of the limit cycle that corresponds to the stable hopping behaviour is wider for higher values of hydrodynamic drag. This would therefore suggest that increasing the frontal area, by means of a morphing body, could enhance the stability of the system. However, experimentally replicating the results of Calisti and Laschi (2018) is not straightforward as increasing the size of the head not only increases drag, but also added mass with consequent effects on all aggregate model parameters as defined in Eq. 2. In the reported experiments, decreasing the distance of the buoy from the robot primarily corresponds to decreasing the momentum generated by buoyant force on the joint of the pivot responsible for the vertical motion of the system. Secondary effects of reduced hydrodynamic drag momentum and added mass contribution were neglected, thus a buoy distance reduction is considered equivalent to a buoyancy reduction in the model. The trends of the locomotion features with respect to buoy distance, as shown in Fig. 7 and Tab.5 are correctly predicted by the model for both head sizes considered, as well as the buoy distance critical for reaching a stable limit cycle. Increasing the head size has two main consequences with theoretically opposite effects on the stability of the hopping behaviour, if we consider the horizontal motion. On one hand, a stabilizing effect is produced by the increment of the exposed area and thus shows an increase of hydrodynamic drag, while on the other hand, an incremented added mass of water is carried by the system with a consequential loss of stability (Calisti and Laschi (2018)) due to an increase in horizontal speed. However, the increase of the inertial term due to the added mass also carries a very powerful stabilizing effect with respect to the vertical motion, which reduces the maximum vertical speeds and also increased the stability due to buoyancy contribution (see the effect of the added mass increase on the a-dimensional aggregate parameters of the model, in SI Appendix). By analysing the model for the tested configuration, it is clear how the basin of attraction of the limit cycle is deeply modified (Fig. 8) with a clear stabilizing effect, as shown during the experiments. Although the exact values of the hydrodynamic parameters would be difficult to be precisely identified for non-regular shapes of the robot and the trajectories exhibited (but this is challenging as well for traditional underwater systems, Antonelli (2006)), and that contributions that were not addressed may be a part of the observed recovery, our results support that a simple low-order mathematical model was capable of predicting the trends induced by morphological changes and the reshaping of the attractor's landscape and locomotion orbit in particular, as shown in Fig. 6 and Fig. 8. It is worth mentioning that experimentally, we observed a dramatic change in behaviour, with 0 successful runs for the small head and 100% of hopping locomotion for big head in what we called morphological induced recovery (see Tab.2 and Tab.3). This very sharp separation could be mostly due to our limited capability of exploring the space of initial conditions. In our case, the small variations on the initial conditions were inevitably attracted by the falling or the hopping behaviour, but specific initial conditions which grant hopping behaviour also to the small head are likely to exist, along with conversely extreme initial conditions that would increase the likelihood of the big head falling. MC is at the base of a new conception of robotics which aims at taking inspiration from nature to create machines for which an *ecological balance* among mechanical design, control, material properties and surrounding environment subsists, Pfeifer et al. (2005). In particular, the exploitation of the natural dynamics of a system has the possibility to dramatically simplify the control task, by reducing it to initiate the jump to the desired basin of attraction. In such a context, it was formalized that a morphological change could alter the landscape of the attractors and thus induce the convergence to a specific behaviour, Füchslin et al. (2013). Notwithstanding of this very elegant formalization, current experimental results appear limited and the utility of switching mode in a realistic scenario is only speculated, Garrad et al. (2018). On the other hand, our present work has considered a system with two clearly different behaviours (i.e. falling or hopping) with explicit applicative significance. In addition, it has highlighted how a morphological change can affect the interaction with the underwater environment. It is also worth noting the relationship between the bounds of the control input of the system, the morphing of the body, and the behaviours. The only control input of the system is represented by the elongation of the leg, which is responsible for compressing the spring during the punting phase and thus injecting energy in the system until the forces acting on the spring eventually balance and lift off occurs. The control law employed consists of elongating the leg at maximum possible velocity whenever the foot is in contact with the ground. With respect to this, it was shown that by increasing the elongation speed, the system goes toward stable trajectories (Calisti and Laschi (2018)), but in the current experiments, the robot was already employing the maximum elongation speed granted by the actuators, and as such, a recovery of stability via modifications of the control was impossible. However, the solution suggested by MC to the control problem is effective, and by increasing the

head size the interaction of the robot with the surrounding fluid changes, there causes a modification of both the limit cycle and its basin of attraction, as shown in Fig. 6, resulting in the recovery of the periodic hopping behaviour, as reported in Tab. 2. This peculiar capability has been referred to as *morphological control* (Garrad et al. (2018); Füchslin et al. (2013)), and could be exploited only by robots with the possibility of altering their morphology or internal mechanical characteristics, such as the novel category of soft robots, Laschi et al. (2016).

Soft robotics is envisioned to grant all new kind of new abilities to robots. As a matter of fact, most mobile soft robots exploit their deformable bodies to either increase performances or to enable particular gaits (Jayaram and Full (2016)), yet often the benefits with respect to their rigid counterparts lie in intrinsic safety (Abidi and Cianchetti (2017)) rather than in quantitative analysis. Some authors argue that the underwater environment could be exploited to highlight the advantages brought by soft bodies (Corucci et al. (2015a); Giorgio-Serchi and Weymouth (2016)) (due to the close relationships between body shape and forces), but results so far have remained mainly in simulation Auerbach and Bongard (2017). The experiments presented in this paper show how, by varying the morphology of the body, measurable advantages can be obtained (beyond the intrinsic safety given by a deformable robot). To the authors' knowledge, while amazing examples of improved speed were obtained via the evolving legs Vujovic et al. (2017), this is the first example of how a single morphological parameter (i.e. the head size) generates a dramatic change of behaviour in an actual legged robot, i.e. falling or hopping. Finally, a number of researchers take into account the direct interaction of underwater vehicles with the seabed by mean of different kinds of limbs, Greiner et al. (1996); Akizono et al. (1997); Jun et al. (2015); Wang et al. (2017). More recent work envision dynamic legged locomotion (jumping Wang et al. (2017), hopping Picardi et al. (2018), and others Arienti et al. (2013)) as a profitable direction toward the improvement of such kind of locomotion. It appears pivotal to investigate such gaits with respect to the common task of sample collections, which can lead to an increase of the overall weight of the robot. In this regard, the results that were presented in Fig. 8 and in Fig.9 can be interpreted as follows. An underwater legged robot is designed to have a specific degree of locomotion stability (8a). Indeed, after the collection of one or more samples (e.g. rocks), it loses stability due to an increment in weight (8b). Such increment can be easily detected by force sensors embedded in the feet and the degree of stability can be restored by means of a morphological change instead of through implementing a change in control policy (8c). So far, only a few underwater robots have exhibited a morphing soft body, but our results suggest that shape related interactions could be exploited to achieve useful behaviours, thus promoting a novel concept for vehicles. Simulations suggests that morphing itself cannot tackle all disturbance, but it can positively affect the natural dynamics so that effectiveness of control strategies could increase (Tab.4). The experiments presented in this work can be seen from the perspective of solving a control problem, with the requirement being the achieving of dynamic stability, or in other words, converging to a periodic hopping trajectory represented by a limit cycle in the state space, as shown in Fig. 6. In a context where shape-dependent forces play a significant role, a desired behaviour (one might say a control requirement) can be obtained by resorting to a morphological change instead of classic control and, despite the challenges in identification, the mathematical modelling of shape-dependent forces can guide such changes. Soft robotics has introduced technologies that can potentially enable unforeseen abilities of robots, eventually leading them outside of the controlled environments of labs. We believe that, to pursue this long term goal, it is fundamental to tap into the expertise of more consolidated disciplines and to adopt a formal approach that aims at applications whereby being soft provides a quantifiable benefit with respect to traditional solutions.

5 Conclusions

In this study, we presented and discussed the experiments on a single leg underwater robot, for which it is possible to obtain stable hopping locomotion through manually increasing the size of a deformable head, and without altering any other property (e.g. buoyancy, mass) or changing the actuation strategy employed. Moreover, we argued that a similar result could not be achieved by a classic control because the actuator was working at maximum capacity. We compared the experimental results with the simulations of a simple mathematical model that described the dynamics of an inverted pendulum featuring a spring in series with a linear actuator subjected to the shape-dependent contributions of the underwater environment, formally characterizing the effects of morphological changes in terms of limit cycle and basin of attraction. Beyond the interest for underwater legged locomotion, the presented results represent experimental evidence that, in a context dominated by shape-dependent forces, show that it is possible to dramatically alter the behaviour of a dynamical system and induce the convergence to a desirable condition by means of a morphing body and that such a strategy is not just an elegant alternative to classic control, but may overcome the problem of actuator saturation.

6 Appendix

A displacement of the buoy dl in the experimental setup can be modelled by adding a dummy volume dV to the volume of the robot V_r. In this section we derive the relation between dV and dl, and in turn the relation between dV and the variation of the aggregate parameter $\tilde{C}$. The schematics in Fig. 10 show the forces that act vertically on the system.

The torque T acting on the system is:

$$T = mgL - \rho_w V_r g L + m_b g l_b - \rho_w V_b g l_b \quad (4)$$

where m_b and V_b are mass and volume of the buoy, respectively. Moving the buoy along the boom by dl alters the torque on the system, which now is:

$$T_1 = mgL - \rho_w V_r g L + m_b g (l_b + dl) - \rho_w V_b g (l_b + dl) \quad (5)$$

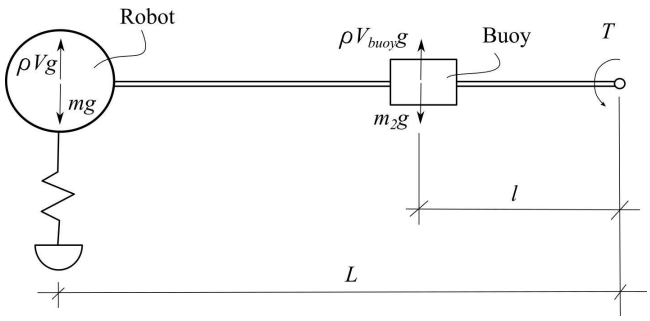

Figure 10. Forces acting vertically on the system: the robot has a fixed arm L for the momentum T with respect to the pivot, while the distance of the buoy l_b can be varied to increase or decrease the overall momentum acting on the system.

Mathematically, an equivalent effect can be obtained by not moving the buoy and adding a massless dummy volume dV to the robot instead. In this case the torque on the system becomes:

$$T_2 = mgL - \rho_w(V_r + dV)gL + m_b g l_b - \rho_w V_b g l_b \quad (6)$$

The relation between dl and dV is found by taking $T_1 = T_2$ and neglecting m_b because the buoy is very light and thus $m_b << \rho_w V_b$. The resulting relation is expressed as:

$$dV = V_b \frac{dl}{L} \quad (7)$$

In turn, by taking the derivative of $\tilde{C}$ (Eq. 2) with respect to V and substituting Eq.7, the variation of aggregate parameter $\tilde{C}$ as function of dl is found as:

$$d\tilde{C} = -\frac{L\rho_w V_b g}{(m+M)} dl \quad (8)$$

References

Abidi H and Cianchetti M (2017) On Intrinsic Safety of Soft Robots. *Frontiers in Robotics and AI* 4(February): 1–6. DOI: 10.3389/frobt.2017.00005.

Akizono J, Tanaka T, Nakagawa K, Tsuji T and Iwasaki M (1997) Seabottom roughness measurement by aquatic walking robot. In: *OCEANS '97. MTS/IEEE Conference Proceedings*, volume 2. pp. 1395–1398 vol.2. DOI:10.1109/OCEANS.1997.624200.

Antonelli G (2006) *Underwater Robots, Motion and Force Control of Vehicle-Manipulator Systems (Springer Tracts in Advanced Robotics)*. New York: Springer.

Arienti A, Calisti M, Giorgio-Serchi F and Laschi C (2013) PoseiDRONE: Design of a soft-bodied ROV with crawling, swimming and manipulation ability. In: *2013 MTS/IEEE OCEANS conference, 23 to 26 September 2013, San Diego (CA)*. pp. 1–7.

Auerbach JE and Bongard JC (2014) Environmental Influence on the Evolution of Morphological Complexity in Machines. *PLoS Comput Biol* 10(1): e1003399.

Blickhan R (1989) The spring-mass model for running and hopping. *Journal of Biomechanics* 22(11/12): 1217–1227.

Bongard J (2011) Morphological change in machines accelerates the evolution of robust behavior. *Proceedings of the National Academy of Sciences* 108(4): 1234–1239. DOI:10.1073/pnas.1015390108.

Brown B and Zeglin G (1998) The bow leg hopping robot. *Proceedings. 1998 IEEE International Conference on Robotics and Automation* 1: 781–786.

Calisti M, Falotico E and Laschi C (2016) Hopping on Uneven Terrains With an Underwater One-Legged Robot. *IEEE Robotics and Automation Letters* 1(1): 461–468. DOI:10.1109/LRA.2016.2521928.

Calisti M and Laschi C (2015) Underwater running on uneven terrain. In: *OCEANS 2015 - Genova*. pp. 1–5. DOI:10.1109/OCEANS-Genova.2015.7271366.

Calisti M and Laschi C (2018) Morphological and control criteria for self-stable underwater hopping Morphological and control criteria for self-stable underwater hopping. *Bioinspiration and Biomimetics* .

Calisti M, Picardi G and Laschi C (2017) Fundamentals of soft robot locomotion. *Journal of The Royal Society Interface* 14(130): 20170101. DOI:10.1098/rsif.2017.0101.

Corucci F, Calisti M, Hauser H and Laschi C (2015a) Evolutionary discovery of self-stabilized dynamic gaits for a soft underwater legged robot. In: *2015 International Conference on Advanced Robotics (ICAR), 27 to 31 July, Istanbul*. pp. 337–344. DOI: 10.1109/ICAR.2015.7251477.

Corucci F, Calisti M, Hauser H and Laschi C (2015b) Novelty-Based Evolutionary Design of Morphing Underwater Robots. In: *Proceedings of the 2015 Annual Conference on Genetic and Evolutionary Computation, 11 to 15 June 2015, Madrid*, GECCO '15. New York, NY, USA: ACM. ISBN 978-1-4503-3472-3, pp. 145–152. DOI:10.1145/2739480.2754686.

Eder M, Hisch F and Hauser H (2017) Morphological computation-based control of a modular, pneumatically driven, soft robotic arm. *Advanced Robotics* 1864(December): 1–11. DOI:10.1080/01691864.2017.1402703.

Table 5. Comparison of locomotion features between small (S) and big (B) head configuration. Values are mean (standard deviation), p-value is reported for every comparison. Values are rounded to two decimal digits for features, and four digits for p-value. The $*$ indicates that the p-value is of inferior order to the four digits.

	v_x [cm/s]		v_y^{lo} [cm/s]		Δy [cm]		f [1/s]	
Buoy Position	S	B	S	B	S	B	S	B
20.5 [cm]	6.31(3.17)	9.43(0.35)	4.64(0.29)	3.83(0.84)	1.58(0.16)	1.90(0.53)	1.04(0.08)	0.86(0.03)
	0.0883		0.0378		0.1151		0.0007	
19.2 [cm]	7.68(0.17)	8.28(0.29)	4.98(0.32)	3.56(0.73)	1.80(0.09)	1.82(0.06)	0.96(0.03)	0.81(0.04)
	0.0020		0.2241		0.3256		0.0001	
17.8 [cm]	7.64(0.12)	7.56(0.23)	4.87(0.32)	4.59(0.73)	1.79(0.14)	2.39(0.37)	0.94(0.02)	0.76(0.03)
	0.2335		0.2241		0.0048		0.0000*	
16.5 [cm]	7.29(0.14)	7.35(0.28)	5.25(0.49)	4.27(0.56)	1.97(0.27)	2.37(0.44)	0.87(0.04)	0.73(0.05)
	0.3495		0.0090		0.0615		0.0008	
15.1 [cm]	5.96(0.72)	6.93(0.24)	5.75(0.28)	4.16(0.45)	2.27(0.13)	2.30(0.30)	0.78(0.03)	0.63(0.02)
	0.0108		0.0001		0.4007		0.0000*	
13.1 [cm]	5.90(0.23)	6.52(0.24)	6.45(0.27)	4.47(0.30)	2.68(0.09)	2.52(0.14)	0.67(0.01)	0.57(0.02)
	0.0016		0.0000*		0.0299		0.0000*	
12.1 [cm]	5.17(0.84)	5.83(0.15)	6.41(0.15)	4.71(0.59)	2.92(0.10)	3.02(0.46)	0.61(0.01)	0.51(0.02)
	0.0603		0.0001		0.3241		0.0000*	
10.6 [cm]	4.91(0.16)	5.12(0.20)	6.93(0.28)	4.84(0.29)	3.31(0.13)	3.56(0.40)	0.54(0.02)	0.43(0.01)
	0.0491		0.0000*		0.1197		0.0000*	
9.5 [cm]	4.40(0.14)	4.49(0.53)	7.28(0.09)	5.22(0.38)	3.94(0.11)	4.24(0.38)	0.46(0.01)	0.39(0.02)
	0.3603		0.0000*		0.0660		0.0000*	

Füchslin RM, Dzyakanchuk A, Flumini D, Hauser H, Hunt KJ, Luchsinger RH, Reller B, Scheidegger S and Walker R (2013) Morphological Computation and Morphological Control: Steps Toward a Formal Theory and Applications. *Artificial Life* 19(1): 9–34. DOI:10.1162/ARTL_a_00079.

Garrad M, Rossiter J and Hauser H (2018) Shaping behaviour with adaptive morphology. *IEEE Robotics and Automation Letters* 3(3): 1–1. DOI:10.1109/LRA.2018.2807591.

Giorgio-Serchi F and Weymouth GD (2016) Drag cancellation by added-mass pumping. *arXiv preprint arXiv:1604.02663* .

Greiner H, Shectman A, Chikyung Won, Elsley R and Beith P (1996) Autonomous legged underwater vehicles for near land warfare. In: *Proceedings of Symposium on Autonomous Underwater Vehicle Technology*. ISBN 0-7803-3185-0, pp. 41–48. DOI:10.1109/AUV.1996.532399.

Guizzo E and Ackerman E (2015) The hard lessons of DARPA's robotics challenge [News]. *IEEE Spectrum* 52(8): 11–13. DOI: 10.1109/MSPEC.2015.7164385.

Hauser H and Corucci F (2017) Morphosistaking morphological computation to the next level. In: *Soft Robotics: Trends, Applications and Challenges*. Springer, pp. 117–122.

Hauser H, Füchslin RM and Nakajima K (2018) Morphological Computation - The Physical Body as Computational Resource. pp. 833–852.

Iida F and Pfeifer R (2004) Cheap rapid locomotion of a quadruped robot: Self-stabilization of bounding gait. *Proceedings of the 8th International Conference on Intelligent Autonomous Systems (IAS-8)*:642–649

Jayaram K and Full RJ (2016) Cockroaches traverse crevices, crawl rapidly in confined spaces, and inspire a soft, legged robot. *Proceedings of the National Academy of Sciences* 113(8): E950—-E957.

Jun Bh, Lee Pm and Jung Yh (2015) Experience on Underwater Artefact Search Using Underwater Walking Robot Crabster CR200. *Oceans 2015 Washington D.C* .

Jun G, Shusheng B, Yicun X and Cong L (2008) Development and design of a robotic Manta Ray featuring flexible pectoral fins. *2007 IEEE International Conference on Robotics and Biomimetics (ROBIO), 15 to 18 December 2007, Sanya* : 519–523DOI:10.1109/ROBIO.2007.4522216.

Laschi C, Mazzolai B and Cianchetti M (2016) Soft robotics: Technologies and systems pushing the boundaries of robot abilities. *Science Robotics* 1(1): eaah3690. DOI:10.1126/scirobotics.aah3690.

Lund H H and Hallam J (1997) Evolving robot morphology. In: *Proceedings of 1997 IEEE International Conference on Evolutionary Computation*. pp. 197–202.

Ma KY, Chirarattananon P, Fuller SB and Wood RJ (2013) Controlled flight of a biologically inspired, insect-scale robot. *Science* 340(6132): 603–607.

Marchese AD, Onal CD and Rus D (2014) Autonomous soft robotic fish capable of escape maneuvers using fluidic elastomer actuators. *Soft Robotics* 1(1): 75–87.

Mautner Craig and Belew Richard K. (2000) Evolving robot morphology and control. *Artificial Life and Robotics* 4(3): 130–136.

Nakajima K, Hauser H, Kang R, Guglielmino E, Caldwell DG and Pfeifer R (2013) A soft body as a reservoir: case studies in a dynamic model of octopus-inspired soft robotic arm. *Frontiers in Computational Neuroscience* 7(July): 1–19. DOI:10.3389/fncom.2013.00091.

Nakajima K, Hauser H, Li T and Pfeifer R (2015) Information processing via physical soft body. *Scientific Reports* 5: 1–11. DOI:10.1038/srep10487.

Nakajima K, Li T, Hauser H and Pfeifer R (2014) Exploiting short-term memory in soft body dynamics as a computational resource. *Journal of The Royal Society Interface* 11. DOI: 10.1098/rsif.2014.0437.

Owaki D, Osuka K and Ishiguro A (2008) On the embodiment that enables passive dynamic bipedal running. *Proceedings - IEEE*

International Conference on Robotics and Automation .

Pfeifer R, Iida F and Bongard J (2005) New robotics: design principles for intelligent systems. *Artif. Life* 11: 99–120.

Pfeifer R, Iida F and Gomez G (2006) Morphological computation for adaptive behavior and cognition. *International Congress Series* 1291: 22–29.

Pfeifer R, Lungarella M and Iida F (2007) Self-Organization, Embodiment, and Biologically Inspired Robotics. *Science* 318(5853): 1088–1093.

Picardi G, Laschi C and Calisti M (2018) Model-based open loop control of a multigait legged underwater robot. in: *Mechatronics 55: 162–170*. DOI:10.1016/j.mechatronics.2018.09.006

Shepherd RF, Ilievski F, Choi W, Morin Sa, Stokes AA, Mazzeo AD, Chen X, Wang M and Whitesides GM (2011) Multigait soft robot. *Proceedings of the National Academy of Sciences* 108(51): 20400–20403. DOI:10.1073/pnas.1116564108.

Sims K (1994) Evolving 3D Morphology and Behavior by Competition. *Artificial Life* 1(4): 353–372.

Vu HQ, Hauser H, Leach D and Pfeifer R (2013) A variable stiffness mechanism for improving energy efficiency of a planar single-legged hopping robot. In: *Advanced Robotics (ICAR), 2013 16th International Conference on*. IEEE, pp. 1–7.

Vujovic V, Rosendo A, Brodbeck L and Iida F (2017) Evolutionary Developmental Robotics: Improving Morphology and Control of Physical Robots.. *Artificial Life* 23(2): 169–185.

Wang G, Chen X, Yang S, Jia P, Yan X and Xie J (2017) Subsea crab bounding gait of leg-paddle hybrid driven shoal crablike robot. *Mechatronics* 48(145): 1–11. DOI:10.1016/j.mechatronics.2017.10.002.

Zhao L, Huang Q, Deng X and Sane SP (2010) Aerodynamic effects of flexibility in flapping wings. *Journal of the Royal Society, Interface / the Royal Society* 7(44): 485–97. DOI:10.1098/rsif.2009.0200.

Zhao Q, Nakajima K, Sumioka H, Hauser H and Pfeifer R (2013) Spine dynamics as a computational resource in spine-driven quadruped locomotion. In: *IEEE International Conference on Intelligent Robots and Systems*. ISBN 9781467363587, pp. 1445–1451. DOI:10.1109/IROS.2013.6696539.